Imaging analysis reveals mechanistic differences between first- and second-phase insulin exocytosis

Mica Ohara-Imaizumi,[1] Tomonori Fujiwara,[2] Yoko Nakamichi,[1] Tadashi Okamura,[5] Yoshihiro Akimoto,[3] Junko Kawai,[1,6] Satsuki Matsushima,[4] Hayato Kawakami,[3] Takashi Watanabe,[4] Kimio Akagawa,[2] and Shinya Nagamatsu[1]

[1]Department of Biochemistry, [2]Department of Cell Physiology, [3]Department of Anatomy, and [4]Department of Clinical Pathology, Kyorin University School of Medicine, Mitaka, Tokyo 181-8611, Japan
[5]Division of Animal Models, Department of Infectious Diseases, Research Institute, International Medical Center of Japan, Tokyo 162-8655, Japan
[6]Department of Medicine, Metabolism and Endocrinology, Juntendo University School of Medicine, Tokyo, 113-8421, Japan

The mechanism of glucose-induced biphasic insulin release is unknown. We used total internal reflection fluorescence (TIRF) imaging analysis to reveal the process of first- and second-phase insulin exocytosis in pancreatic β cells. This analysis showed that previously docked insulin granules fused at the site of syntaxin (Synt)1A clusters during the first phase; however, the newcomers fused during the second phase external to the Synt1A clusters. To reveal the function of Synt1A in phasic insulin exocytosis, we generated Synt1A-knockout (Synt1A$^{-/-}$) mice.

Synt1A$^{-/-}$ β cells showed fewer previously docked granules with no fusion during the first phase; second-phase fusion from newcomers was preserved. Rescue experiments restoring Synt1A expression demonstrated restoration of granule docking status and fusion events. Inhibition of other syntaxins, Synt3 and Synt4, did not affect second-phase insulin exocytosis. We conclude that the first phase is Synt1A dependent but the second phase is not. This indicates that the two phases of insulin exocytosis differ spatially and mechanistically.

Introduction

Glucose-stimulated insulin release displays a biphasic pattern in both in vitro and in vivo systems (Curry et al., 1968; Rorsman et al., 2000). This pattern consists of a rapidly initiated and transient first phase preceding a sustained second phase. The ability of glucose to evoke first-phase release is shared by other stimuli (such as high KCl stimulation), resulting in membrane depolarization followed by increased cytosolic Ca^{2+}, whereas only fuel secretagogues are able to initiate second-phase insulin release (Henquin, 2000). Electrophysiological experiments in single β cells have shown that first-phase release reflects Ca^{2+}-dependent exocytosis of primed granules in a readily releasable pool of granules, whereas second-phase release involves an ATP-dependent release of granules that may be located further from the release site in a reserve pool (Rorsman et al., 2000; Rorsman and Renstrom, 2003). These results suggest that the two phases

of release subject insulin granules to nonsynonymous regulatory mechanisms.

Fundamental components of secretory machinery, such as SNARE, required for the docking and fusion of vesicles in neuronal cells (Südhof, 2004), are expressed in pancreatic β cells and play an important role in insulin exocytosis (Nagamatsu et al., 1996; Wheeler et al., 1996; Nagamatsu et al., 1999). Although the function of SNAREs in docking and fusion during exocytosis is already established (Jahn et al., 2003; Südhof, 2004), the distinct role of SNAREs in the individual phases of insulin release remains unclear.

Interestingly, the expression of t-SNARE, syntaxin 1A/HPC-1 (Synt1A; Bennett et al., 1992; Inoue et al., 1992), and its cognate SNARE partners, synaptosome-associated protein of 25 kD (SNAP-25) and vesicle-associated membrane protein 2 (VAMP2), reportedly decreased in islets of the Goto-Kakizaki rat, an animal model for human type 2 diabetes (Nagamatsu et al., 1999; Gaisano et al., 2002; Zhang et al., 2002), and in type 2 diabetic patients (Ostenson et al., 2006). Because type 2 diabetes is associated with disturbances in the release pattern manifested as the selective loss of first-phase release (Ward et al., 1984; O'Rahilly et al., 1986; Cerasi, 1994), SNAREs may have

a specialized role in phasic insulin exocytosis. In the present study, we used Synt1A$^{-/-}$ mice and total internal reflection fluorescence (TIRF) imaging to investigate a potential role for Synt1A in first-phase insulin release. Synt1A$^{-/-}$ pancreatic β cells displayed no fusion from previously docked granules in first-phase release, whereas fusion from newcomers, which are responsible for second-phase release, was still preserved. Thus, we propose a new model for biphasic insulin release wherein docking and fusion of insulin granules is Synt1A dependent during the first phase but Synt1A independent during the second phase.

Results

Interaction between insulin granules and Synt1A during biphasic insulin release

We initially analyzed the dynamic interaction between insulin granules and Synt1A in control mouse β cells using dual-color TIRF microscopy (TIRFM). Expression of GFP-tagged insulin allowed insulin granule observation, and Synt1A was detected by a TAT-conjugated Cy3-tagged mAb. Here, we chose not to use a conventional overexpression approach, such as Synt1A tagged with GFP or RFP, because overexpression of syntaxin disturbs

the function of endogenous syntaxin molecules (Nagamatsu et al., 1996). Therefore, to analyze the interaction between insulin granules and Synt1A clusters during biphasic insulin release, we labeled the endogenous Synt1A clusters with TAT antibody. As previously reported (Ohara-Imaizumi et al., 2004a), TAT-conjugated Cy3-labeled anti-Synt1A antibody was rapidly transduced into living β cells (unpublished data). We ensured that TAT-conjugated Cy3-labeled anti-Synt1A antibody specifically labeled endogenous Synt1A clusters in the plasma membrane. Cells treated with TAT-conjugated Cy3 anti-Synt1A mAb for 50 min were fixed and immunostained with anti-Synt1A pAb. As shown in Fig. S1 (available at http://www.jcb.org/cgi/content/full/jcb.200608132/DC1), there was overlapping of Synt1A clusters labeled with TAT-conjugated Cy3 anti-Synt1A mAb (red) and those stained with anti-Synt1A pAb (green). In addition, it should be noted that most endogenous Synt1A was labeled with TAT antibody.

Pancreatic β cells that expressed insulin-GFP (Fig. S1, green) and were treated with TAT-conjugated Cy3 anti-Synt1A antibody (red) were stimulated by 22 mM glucose. Dual-color TIRF images were obtained every 300 ms (Fig. 1 A). Approximately 75% of insulin granule fusion during the first phase (<4 min after stimulation) involved previously docked rather
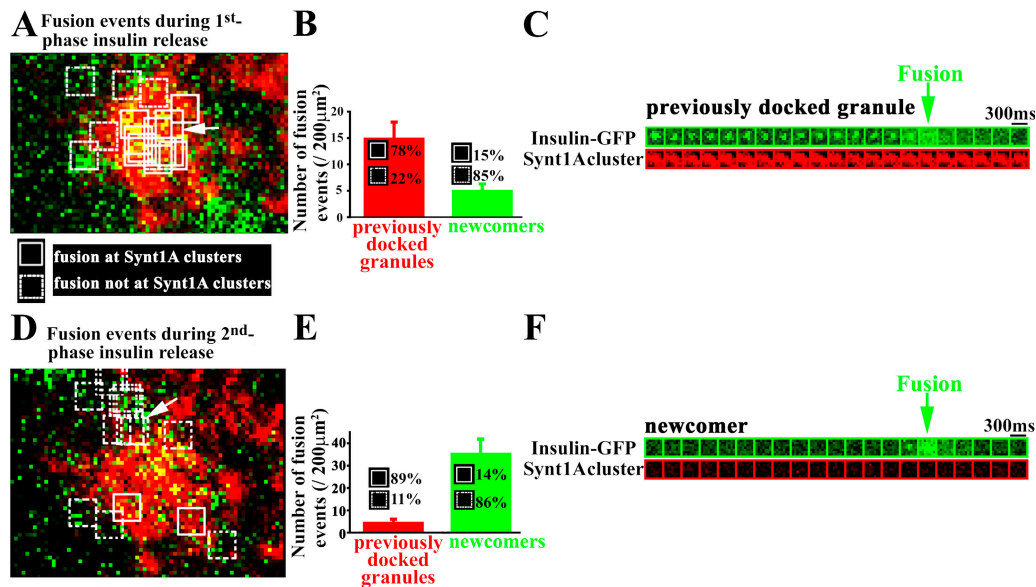
Figure 1. **Dual-color TIRFM of dynamic interaction between docking and fusing GFP-tagged insulin granules and Cy3-labeled Synt1A clusters in glucose-induced insulin release in control mouse β cells.** 2 d after β cells were infected with the vector expressing insulin-GFP (green), cells were treated with TAT-conjugated Cy3-labeled anti-Synt1A antibody (red) for 50 min. Images were recorded for GFP-tagged insulin granules (green) and Cy3-labeled Synt1A clusters (red) simultaneously (300-ms intervals). (A) Sites of insulin granule fusion events during first-phase release under 22 mM glucose stimulation (0–4 min after glucose stimulation). Solid boxes (1 × 1 μm) represent the sites of fusion events at Synt1A clusters. Dashed boxes indicate the sites of fusion events not at Synt1A clusters (Video 1, available at http://www.jcb.org/cgi/content/full/jcb.200608132/DC1). (B) Analysis of fusion events during first-phase release (n = 5 cells). The fused granules are divided into two categories, fusion from previously docked granules (red) and newcomers (green). Previously docked granule indicates that the morphologically previously docked granule is fused with the plasma membrane. Newcomer indicates that the granule approaches from the inside (being absent before stimulation), reaches the plasma membrane, and quickly fuses. As previously reported (Ohara-Imaizumi et al., 2004b), ~75% of insulin granule fusion during the first phase was from previously docked granules, and the remaining was from newcomers. Most fusion from previously docked granules occurred at Synt1A clusters (78.1 ± 4.0% of all fusion from previously docked granules); fusion from newcomers occurred external to Synt1A clusters (85.0 ± 2.9% of all fusion from newcomers) during the first phase. Data are mean ± SEM. (C) Sequential images (1 × 1 μm, 300-ms intervals; A, box indicated by arrow) of fusion from previously docked granules (green) at the Synt1A cluster (red) during the first phase. (D) Sites of insulin granule fusion during second-phase insulin release (>5 min after glucose stimulation; Video 2). Solid and dashed boxes are as described above. (E) Analysis of fusion events during second-phase release, with fusion occurring mostly from newcomers (Ohara-Imaizumi et al., 2004b), and at sites distinct from Synt1A clusters (86.1 ± 1.2% of all fusion from newcomers; n = 5 cells). Data are mean ± SEM. (F) Sequential images (1 × 1 μm, 300-ms intervals; D, box indicated by arrow) of fusion from newcomers (green) external to Synt1A clusters (red) during the second phase.

than newcomer granules (Fig. 1 B). We observed that most fusion events involving previously docked granules occurred at the site of Synt1A clusters (Fig. 1, B and C), whereas fusion from newcomers occurred at sites distinct from the Synt1A clusters. There was no significant difference in the number of fusion events between control (see Fig. 3 B) and TAT-conjugated Cy3 anti-Synt1A mAb–treated β cells (Fig. 1 A): the total number of fusion events from previously docked granules in wild-type (WT) versus TAT-treated cells was 18.2 ± 1.8 versus 14.9 ± 3.1 in 0–4 min (P = NS; $n > 5$ cells), suggesting that the introduction of TAT-conjugated Cy3 anti-Synt1A mAb into β cells does not affect insulin exocytosis. These results suggest that first-phase release heavily involves a Synt1A-based SNARE complex, whereas second-phase release is chiefly independent of a Synt1A-based SNARE complex.

Morphometric analysis of insulin granules in Synt1A$^{-/-}$ mice

If Synt1A is essential for docking and fusing insulin granules specifically during the first phase, the deletion of Synt1A may cause reduction in first-phase but not second-phase insulin release. To examine this hypothesis, we used β cells from Synt1A$^{-/-}$ mice (Fujiwara et al., 2006) as a context for analyzing docking and fusion of insulin granules by TIRFM. We first investigated Synt1A protein levels in Synt1A$^{-/-}$ versus WT mouse pancreatic islets. Fig. S2 (available at http://www.jcb.org/cgi/content/full/jcb.200608132/DC1) shows the lack of Synt1A protein expression in Synt1A$^{-/-}$ islets. Expression of Synt1B was not observed in either Synt1A$^{-/-}$ or WT islets, in accord with the report that Synt1B is expressed at very low levels in control β cells (Nagamatsu et al., 1996), although the brain abundantly expresses Synt1B (Bennett et al., 1992). We found no difference between WT and Synt1A$^{-/-}$ islets in expression levels of other plasma membrane proteins, such as Synt3, Synt4, the other SNAREs, and related proteins SNAP-25, VAMP2, and Munc18. We then examined the pancreatic islets morphologically (Fig. S3). We found that paraffin-embedded pancreatic tissue sections showed insulin immunofluorescence patterns typical for β cells with no notable difference between the Synt1A$^{-/-}$ and WT islets (Fig. S3, A and B). EM of pancreatic β cells also revealed that cell size, total number of granules per section, and mean granule diameter were similar between WT and Synt1A$^{-/-}$ β cells (Fig. S3, C–F). Thus, Synt1A$^{-/-}$ β cells displayed specific Synt1A protein depletion but were similar to WT cells in these other traits assayed.

Docking status of insulin granules in Synt1A$^{-/-}$ β cells

We examined the docking status of insulin granules in Synt1A$^{-/-}$ β cells using TIRFM with immunostaining for insulin (Fig. 2 A). Because evanescent field illumination reaches a <100-nm-thick layer immediately adjacent to the cover glass under our TIRF conditions, TIRFM illuminates only the plasma membrane with its associated organelles, such as synaptic vesicles (Zenisek et al., 2000), secretory granules (Parsons et al., 1995), and glucose transporter 4 (GLUT4) vesicles (Lizunov et al., 2005), where a cell adheres tightly to the cover glass. We interpret the individual

fluorescent spots shown in the TIRF image in Fig. 2 A to be equivalent to morphologically docked granules (see Materials and methods). We rarely observed morphologically docked granules in Synt1A$^{-/-}$ β cells (number of docked granules: 253.3 ± 10.2 vs. 12.3 ± 2.2 granules per 200 μm^2 in WT and Synt1A$^{-/-}$ β cells, respectively; $n = 12$ cells; P < 0.0001). Plasma membrane staining with a lipophilic dye ensured that the Synt1A$^{-/-}$ β cells adhered tightly to the cover glass (unpublished data).

To confirm the TIRFM data, we used EM to examine insulin granules that were morphologically docked to the plasma membrane. Using EM, granules at their shortest distance of <10 nm from the plasma membrane qualified as morphologically docked granules (Parsons et al., 1995; Fig. 2 B). The number of morphologically docked granules observed by EM was significantly reduced in Synt1A$^{-/-}$ β cells (9.6 ± 1.5 vs. 0.8 ± 0.2 granules per 10 μm of plasma membrane in WT and Synt1A$^{-/-}$ cells, respectively; $n = 12$ cells; P < 0.0001). Along with the results of the morphometric analysis, these data suggest that Synt1A deficiency specifically impairs the docking of insulin granules to the plasma membrane.
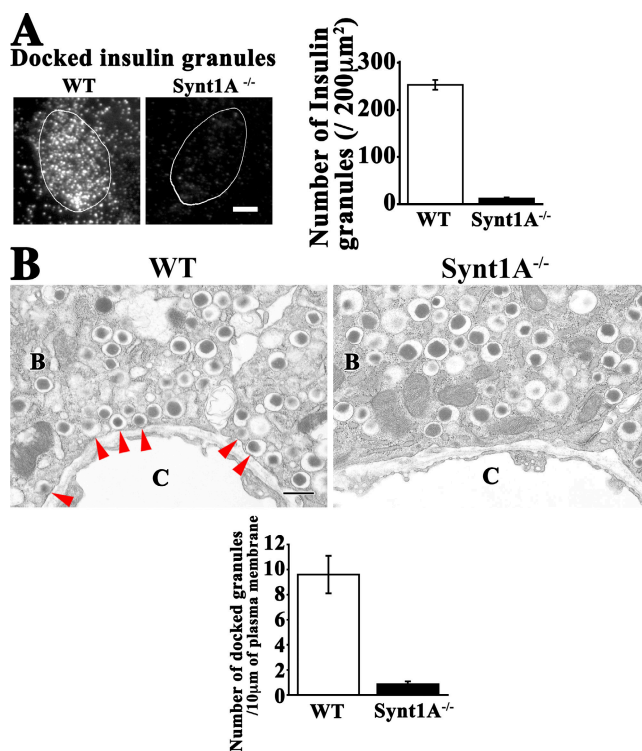
Figure 2. **Synt1A deficiency impairs docking of insulin granules to the plasma membrane in pancreatic β cells.** (A) TIRFM of insulin granules morphologically docked to the plasma membrane. (left) Typical TIRF images of docked insulin granules in WT or Synt1A$^{-/-}$ β cells. The surrounding lines represent the outline of cells that attached to the cover glass. Bar, 5 μm. Pancreatic β cells were prepared from WT and Synt1A$^{-/-}$ mice, fixed, and immunostained for insulin. (right) Number of insulin granules morphologically docked to the plasma membrane. Individual fluorescent spots shown in TIRF images were manually counted per 200 μm^2; $n = 15$ cells. (B) Electron micrograph of β cell sections. (top) Typical EM images of the plasma membrane area facing the blood capillary (C) of WT and Synt1A$^{-/-}$ β cells (B). Bar, 500 nm. (bottom) Number of morphologically docked insulin granules per 10 μm of plasma membrane. Granules at their shortest distance of <10 nm from the plasma membrane were qualified as morphologically docked granules (red arrowheads). Results are provided as the mean ± SEM.
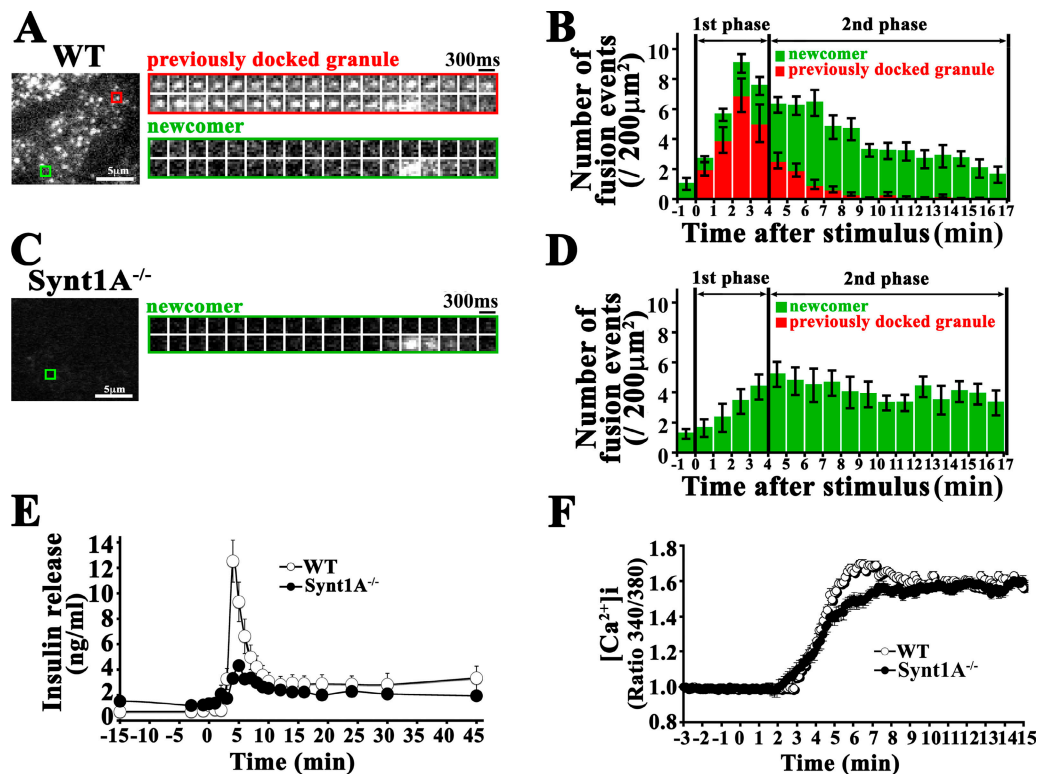
Figure 3. **Effects of Synt1A deficiency on glucose-induced biphasic insulin release.** (A) TIRFM of single insulin granule motion in WT β cells under 22 mM high glucose stimulation (Video 3, available at http://www.jcb.org/cgi/content/full/jcb.200608132/DC1). Red and green boxes indicate that the granules to be fused with the plasma membrane originated from previously docked (red) or newcomer (green) granules. Sequential images (1 μm × 1 μm; 300-ms intervals) of docking and fusion from the previously docked granules (red box) and the newcomers (green box) are presented. (B) Histogram of the number of fusion events (per 200 μm^2) in WT β cells at 60-s intervals after stimulation (n = 10 cells). The red column shows fusion from previously docked granules, and the green column shows fusion from newcomers. During the first phase, fusion occurred mostly from previously docked granules. The fusing granules during the second phase originated mostly from newcomers. (C) TIRFM during glucose stimulation in Synt1A$^{-/-}$ β cells (Video 4) and sequential images of a newcomer granule docking and fusing (green box) under glucose stimulation. (D) Histogram of the number of fusion events (per 200 μm^2) in the Synt1A$^{-/-}$ cells at 60-s intervals after stimulation (n = 10 cells). (E) Glucose-induced insulin release from perfused WT and Synt1A$^{-/-}$ β cells stimulated with 22 mM glucose. The cells in the cell chamber (∼5 × 10^5 cells per chamber) were perfused with KRB (0.5 ml/min) at 37°C, and the perfusate was analyzed for insulin by ELISA. (F) 22 mM glucose-induced changes in [Ca^{2+}]$_i$ in WT and Synt1A$^{-/-}$ β cells. Changes in [Ca^{2+}]$_i$ were measured by 2 μM Fura-2 AM. Time 0 indicates when the high glucose was added. The fluorescence ratio (340/360) at time 0 was taken as 1. Results are provided as the mean ± SEM.

Effects of Synt1A ablation on insulin exocytosis

We explored the effects of Synt1A deficiency on the dynamic motion of single insulin granules. In agreement with what has been reported for rat β cells (Ohara-Imaizumi et al., 2004b), we found that in WT mouse β cells, fusion of insulin granules with the plasma membrane during first-phase release mainly involved previously docked granules (Fig. 3, A and B; and Video 3, available at http://www.jcb.org/cgi/content/full/jcb.200608132/DC1). In contrast, because Synt1A$^{-/-}$ β cells have fewer docked granules, TIRF analysis in these cells showed that the fusion from previously docked granules was severely abolished (Fig. 3, C and D; and Video 4). Despite an appreciable number of fusion events from previously docked granules in WT β cells, there was no fusion from previously docked granules in Synt1A$^{-/-}$ β cells (18.2 ± 1.8 vs.0 in 0–4 min, WT vs. Synt1A$^{-/-}$; Fig. 3, B and D). However, some fusion from newcomer granules was observed during the first phase even in Synt1A$^{-/-}$ β cells. During second-phase release (>4 min), there was no significant difference in the total number of newcomer fusion events between WT and Synt1A$^{-/-}$ β cells (WT, 43.1 ± 5.0, and Synt1A$^{-/-}$, 49.8 ± 3.7, during 4–17 min; P = NS; n = 10 cells; Fig. 3, B and D). ELISA data evaluating endogenous insulin release from perfused WT and Synt1A$^{-/-}$ β cells (Fig. 3 E) were compatible with the TIRFM data. The small peak of first-phase release from Synt1A$^{-/-}$ β cells shown in perfusion analysis is inferred to be composed of fusion from newcomers. Both the amplitude and time course of the glucose-induced rise in intracellular Ca^{2+} concentration ([Ca^{2+}]$_i$) measured using Fura-2 were similar between WT and Synt1A$^{-/-}$ β cells (Fig. 3 F), suggesting that glucose metabolism and ATP production were normally processed in Synt1A$^{-/-}$ β cells and that Synt1A does not affect the activity of the L-type Ca^{2+} channels. This disagrees with the results of other groups (Yang et al., 1999; Kang et al., 2002; Lam et al., 2005), but the reason for the discrepancy is unknown.

Restoration of Synt1A expression in β cells of Synt1A$^{-/-}$ mice

We performed rescue experiments to confirm Synt1A function in the docking and fusing of granules during first-phase release.

A Syntaxin1A clusters

Synt1A$^{-/-}$
WT   Ax-Cont   Ax-Synt1A

B SNAP-25 clusters

Synt1A$^{-/-}$
WT   Ax-Cont   Ax-Synt1A

C Docked insulin granules

Synt1A$^{-/-}$
WT   Ax-Cont   Ax-Synt1A

D Synt1A$^{-/-}$ β cells

Ax-Cont-infected

Ax-Synt1A-infected

E Fusion events during 1st-phase insulin release

☐ fusion at Synt1A clusters
☐ fusion not at Synt1A clusters

F Fusion events during 2nd-phase insulin release
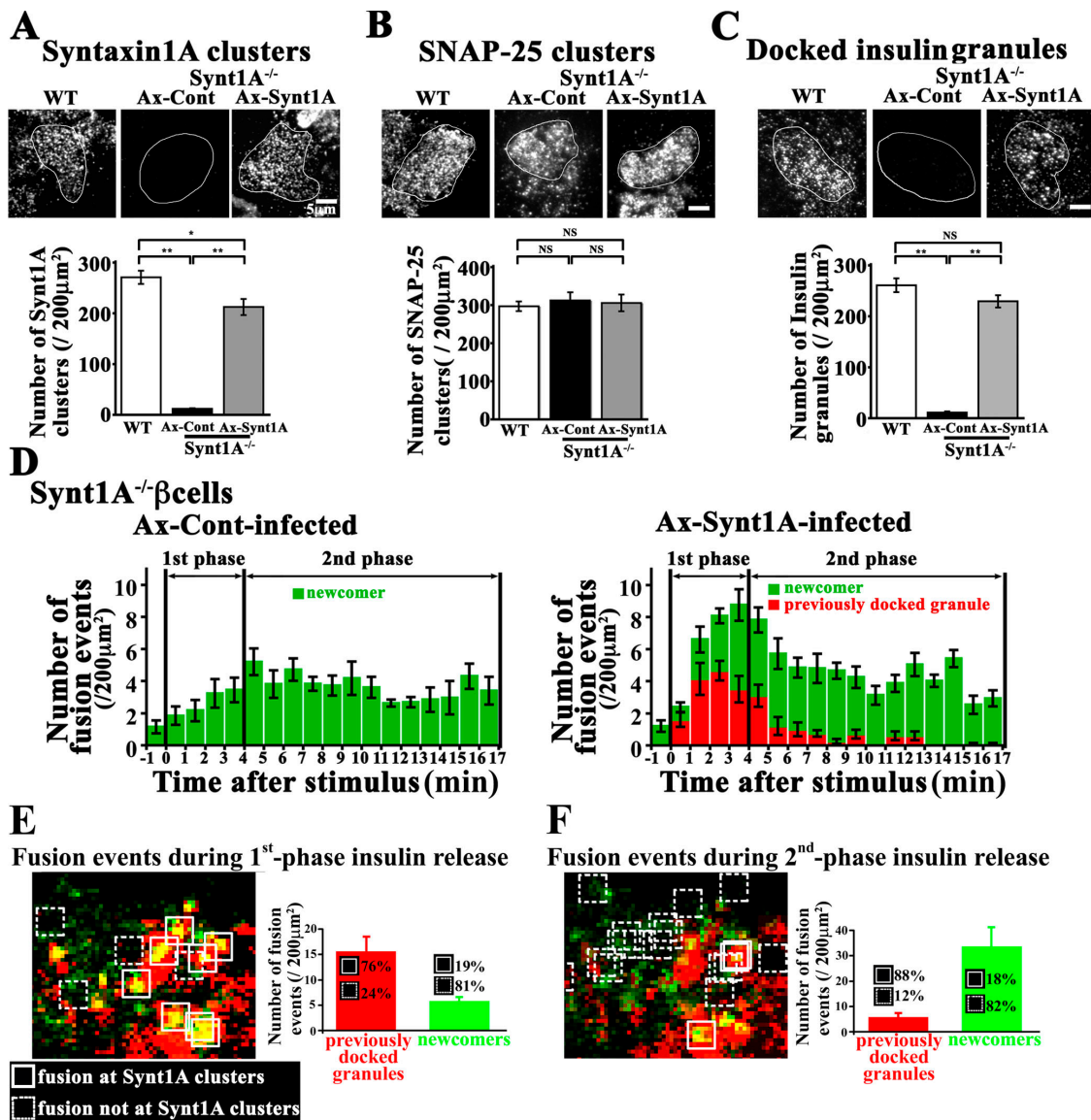
Figure 4. **Rescue of the number of docked insulin granules and fusion events by restoring Synt1A clusters to normal levels in Synt1A$^{-/-}$ β cells.** (A–C) TIRF images and the quantitation of Synt1A clusters (A), SNAP-25 clusters (B), and docked insulin granules (C) on the plasma membrane in WT or Synt1A$^{-/-}$ β cells. Synt1A$^{-/-}$ cells were infected with empty virus Adex1w (Ax-Cont) or with Adex1CA Synt1A (Ax-Synt1A). Cells were fixed and immunostained for Synt1A (A), SNAP-25 (B), and insulin (C). (top) Typical TIRF images. Surrounding lines represent the outline of cells attached to the cover glass. Bars, 5 μm. (bottom) Number of Synt1A (A) and SNAP-25 (B) clusters and docked insulin granules (C) on the plasma membrane. Individual fluorescent spots in TIRF images were manually counted per 200 μm². Data are mean ± SEM (*, P < 0.05; **, P < 0.0001; n = 15 cells). (D) Rescue of fusion events in Synt1A$^{-/-}$ β cells. Synt1A$^{-/-}$ cells were infected with Adex1CA insulin GFP and then Ax-Cont or Ax-Synt1A. The histogram shows the number of fusion events (per 200 μm²) at 60-s intervals after high glucose stimulation. A marked increase in fusion events from previously docked granules was observed in the Synt1A$^{-/-}$ cells infected with Ax-Synt1A relative to Ax-Cont–infected cells. (E) Dual-color TIRFM of docking and fusing GFP-tagged insulin granules (green) and Synt1A clusters labeled with TAT-conjugated Cy3-labeled anti-Synt1A antibody (red) in glucose-induced release from Ax-Synt1A–infected Synt1A$^{-/-}$ cells. Most fusion from previously docked granules occurred at Synt1A clusters (76% of all fusion from previously docked granules); fusion from newcomers occurred external to Synt1A clusters (81% of all fusion from newcomers) during the first phase. Data are mean ± SEM (n = 5 cells). Solid boxes (1 μm × 1 μm) represent the sites of fusion events at the Synt1A clusters. Dashed boxes indicate the sites of fusion events external to the Synt1A clusters. (F) Sites of insulin granule fusion during second-phase insulin release (>4 min after glucose stimulation). Fusion events during second-phase release occurred mostly from newcomers and at sites distinct from Synt1A clusters (82% of all fusion from newcomers; n = 5 cells). Data are mean ± SEM. Solid and dashed boxes are as described above.

We restored Synt1A protein expression to Synt1A$^{-/-}$ β cells by infecting them with an adenovirus encoding Synt1A, Adex1CA Synt1A (Ax-Synt1A; Fig. 4 A). The number of Synt1A clusters was considerably restored, although to still subnormal levels (270.8 ± 13.0 vs. 212.4 ± 15.7, WT vs. Ax-Synt1A–infected Synt1A$^{-/-}$ cells; P < 0.05). In accordance with restored Synt1A

cluster levels, the number of docked insulin granules in Ax-Synt1A–infected Synt1A$^{-/-}$ cells was restored (261.1 ± 13.6 vs. 230.0 ± 12.0, WT vs. Ax-Synt1A–infected Synt1A$^{-/-}$ cells; P = NS). Infection of Adex1CA Synt1A did not alter the number of SNAP25 clusters (Fig. 4 B) that interact with Synt1 clusters (Lang et al., 2002). We then performed TIRFM analysis of

the docking and fusion of insulin granules stimulated by 22 mM glucose in Ax-Synt1A–infected Synt1A$^{-/-}$ β cells. This analysis showed a substantial increase in fusion events from previously docked granules (Fig. 4 D and Video 5, available at http://www.jcb.org/cgi/content/full/jcb.200608132/DC1). The total number of fusion events from previously docked granules during the first phase in Ax-Synt1A–infected Synt1A$^{-/-}$ β cells was restored (18.2 ± 1.8 vs. 12.7 ± 3.3 in 0–4 min, WT vs. Ax-Synt1A–infected Synt1A$^{-/-}$ cells; P = NS). Synt1A restoration did not affect fusion events from newcomers during the second phase. In addition, we examined the interaction between insulin granules and Synt1A clusters labeled with TAT-conjugated Cy3 anti-Synt1A mAb in Ax-Synt1A–infected Synt1A$^{-/-}$ cells. Dual-color TIRFM showed that previously docked granules fused at the site of the Synt1A clusters during the first phase; during the second phase, newcomer granules fused external to the Synt1A clusters (Fig. 4, E and F). This was also observed in WT β cells. These data support a model where Synt1A clusters are required for previously docked granules to dock and fuse during the first phase but dispensable for newcomers to dock and fuse during the second phase.

Other plasma membrane syntaxins assayed are not involved in second-phase release

As shown in Fig. 3 D, the fusion of newcomers during the second phase was well preserved in the absence of Synt1A. Yet the question remained of whether other syntaxin isoforms might be functioning in second-phase release, as pancreatic β cells do express detectable levels of plasma membrane–localized syntaxin isoforms, such as Synt3 and -4 (Jacobsson et al., 1994; Wheeler et al., 1996). To investigate whether these membrane syntaxins Synt3 and -4 are involved in the second phase, we used TAT fusion proteins that encode the Synt3-H3 (TAT-Synt3-H3) and Synt4-H3 (TAT-Synt4-H3) domains. We previously reported that the recombinant Synt1A SNARE motif (H3 domain) fused to TAT (TAT-Synt1A-H3) rapidly transduced into MIN6 β cells, inhibiting insulin release (Ohara-Imaizumi et al., 2002b). Because the syntaxin H3 domain contributes to one of the four α-helical bundles in the SNARE core complex (Jahn and Südhof, 1999), a large molar excess of the Synt1A-H3 domain fused to TAT interrupted the formation of functional SNARE complexes (Ohara-Imaizumi et al., 2002b), as previously reported in other systems (Zhong et al., 1997; O'Connor et al., 1997). We therefore used TAT-H3 of each syntaxin isoform to perform dominant-negative type experiments.

We first produced TAT fusion proteins encoding the Synt3-H3 (TAT-Synt3-H3) and Synt4-H3 (TAT-Synt4-H3) domains. In addition, we produced TAT fusion proteins that encoded the Synt1A-H3 (TAT-Synt1A-H3) and Synt1B-H3 (TAT-Synt1B-H3) domains. A non–coiled-coil domain of ELKS, which has no effect on insulin exocytosis, composed the peptide fusion in our TAT-Control (Ohara-Imaizumi et al., 2005). As shown in Fig. 5 (C and D), the transduction of TAT-Synt3-H3 and TAT-Synt4-H3 into WT β cells reduced the number of fusion events from
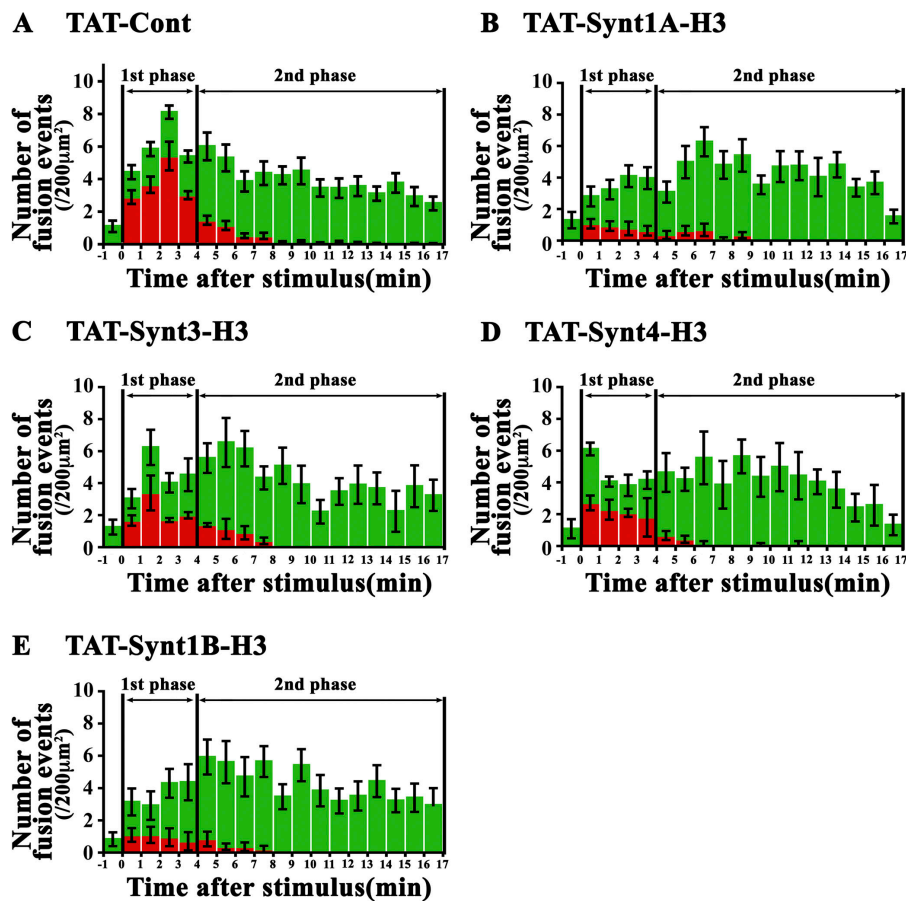
Figure 5. **TIRFM of fusion of GFP-tagged insulin granules in biphasic insulin release from WT β cells treated with TAT-syntaxin-H3.** WT cells expressing GFP-tagged insulin were treated with or without 70 mg/ml of TAT-Cont (A), TAT-Synt1A-H3 (B), TAT-Synt3-H3 (C), TAT-Synt4-H3 (D), or TAT-Synt1B-H3 (E) fusion protein for 50 min, and TIRF images were acquired every 300 ms by 22 mM glucose stimulation. The histogram shows the number of fusion events (n = 10 cells each) at 1-min intervals after high glucose stimulation in the TAT fusion protein–treated cells. The red column shows the fusion from previously docked granules, and the green column shows fusion from newcomers. Data are mean ± SEM.

previously docked granules during the first phase to ∼58 and ∼59% that of control levels, respectively. Second-phase release, which consisted mostly of newcomers, was unaffected by the Synt3-H3 and Synt4-H3 constructs expressed. TAT-Control treatment had no effect on either phase (Fig. 5 A). However, TAT-Synt1A-H3 treatment strongly reduced the total number of fusion events from previously docked granules during the first phase to ∼23% that of control levels, while showing no effect on second-phase release (Fig. 5 B). These data are consistent with our results from Synt1A$^{-/-}$ β cells. Synt1B does not express in β cells, but TAT-Synt1B-H3 treatment showed results similar to those in the TAT-Synt1A-H3 treatment, reducing the total number of fusion events from previously docked granules during the first phase to ∼28% that of control levels (Fig. 5 E). This may be a reflection of a higher homology of Synt1B-H3 to Synt1A-H3. Overall, these findings suggest that these other syntaxin family members are not involved in second-phase release.

Synt1A ablation results in impaired glucose tolerance

Because Synt1A$^{-/-}$ β cells exhibit reduced first-phase insulin release, these mice would be expected to develop diabetes. The Goto-Kakizaki rat model for human type 2 diabetes is known to be defective in first-phase insulin release and displays hyperglycemia (Ostenson et al., 1993). In contrast, we found that Synt1A$^{-/-}$ mice did not show any significant hyperglycemia; fasting blood glucose levels of Synt1A$^{-/-}$ mice were not different from those of WT mice (Synt1A$^{-/-}$, 63.9 ± 4.3 mg/dl [$n = 7$], vs. WT, 65.1 ± 3.3 mg/dl [$n = 11$]; P = NS). However, the oral glucose tolerance test did show impaired glucose tolerance in Synt1A$^{-/-}$ mice (Fig. 6 A). 30 min after challenge, blood glucose levels in Synt1A$^{-/-}$ mice were significantly higher than in WT mice (Synt1A$^{-/-}$, 385.0 ± 14.1 mg/dl [$n = 7$], vs. WT, 286.3 ± 10.4 mg/dl [$n = 11$]; P < 0.0001). In agreement with these data, we found serum insulin levels to be lower in Synt1A$^{-/-}$ than in WT mice at 30 min after challenge (Fig. 6 B). Thus, Synt1A$^{-/-}$ mice displayed an impaired glucose tolerance but not marked hyperglycemia.

Discussion

Our dual-color TIRFM approach has shown that during first-phase release insulin granules fuse at the site of Synt1A clusters, but during second-phase release the granules fuse external to Synt1A clusters. We previously found that granules fusing during the first phase originated mostly from morphologically previously docked granules, whereas granules fusing during the second phase arose from newcomers that were originally stored intracellularly (Ohara-Imaizumi et al., 2004b). We also reported that previously docked insulin granules were colocalized with Synt1A clusters in the plasma membrane of MIN6 β cells (Ohara-Imaizumi et al., 2004a). Collectively, these findings suggested that Synt1A is probably essential for docking and fusing insulin granules during the first phase; however, no direct evidence existed to verify this. Recently, it was reported that other isoforms of the syntaxin family might be associated with

biphasic insulin release (Saito et al., 2003; Spurlin and Thurmond, 2006). We therefore used Synt1A$^{-/-}$ mice to directly address how Synt1A functions in granule docking and fusing in biphasic insulin exocytosis.

First, we examined the docking status of insulin granules in Synt1A$^{-/-}$ β cells. TIRFM and EM analysis in Synt1A$^{-/-}$ β cells documented a marked reduction of the number of granules docked onto the plasma membrane. Because granules fused during the first phase originated from docked granules, as expected, TIRFM revealed that there was no fusion from docked granules during the first phase in knockout cells. However, fusion from newcomers was still preserved in Synt1A$^{-/-}$ β cells under glucose stimulation. Consistent with these data, perfusion analysis of Synt1A$^{-/-}$ β cells showed a marked reduction in first-phase insulin release but no change in second-phase release. Furthermore, restoration of Synt1A to subnormal levels via the adenoviral vector in Synt1A$^{-/-}$ β cells restored the insulin granules docked onto the plasma membrane, accompanied by an appreciable number of fusion events from these granules. Thus, our data provide direct evidence that Synt1A is essential for docking and fusion of insulin granules during first-phase release. The docking status of synaptic vesicles in the brain hippocampus showed no difference between WT and Synt1A$^{-/-}$ mice (Fujiwara et al., 2006). The reason for this discrepancy between brain and pancreatic β cells is unknown, but it may be due to the expression of Synt1B, which is highly homologous to Synt1A and is abundant in brain cells (Bennett et al., 1992) but not in pancreatic β cells (Nagamatsu et al., 1996). Although the function of Synt1B may not be equal to that of Synt1A in pancreatic β cells (Nagamatsu et al., 1996), the brain may have either a tremendous safety network or a different system from pancreatic β cells that permits Synt1B or other homologues to compensate for the lack of Synt1A in brain tissue.

Although our data specify a requirement for Synt1A during first-phase release, we still do not know whether other isoforms of the syntaxin family participate in the first phase. WT β cells transduced with TAT-Synt3-H3 and TAT-Synt4-H3, which function in a dominant-negative manner to the corresponding syntaxin isoforms, showed reduction to some extent in the fusion events from previously docked granules during the first phase (Fig. 5). Yet, as no docked insulin granules were seen on
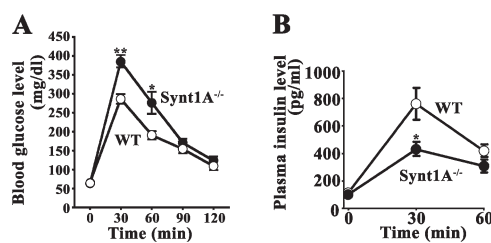
Figure 6. **Glucose tolerance test in WT and Synt1A$^{-/-}$ mice.** (A) Oral glucose tolerance was tested in WT ($n = 11$) and Synt1A$^{-/-}$ ($n = 7$) mice. Blood glucose levels were measured at the indicated times after glucose challenge at 2 g glucose/kg body weight ($n = 6$ each; *, P < 0.005; **, P < 0.0001). (B) Plasma insulin levels were measured in WT and Synt1A$^{-/-}$ mice during the oral glucose tolerance test at the indicated times. Results are provided as the mean ± SEM.
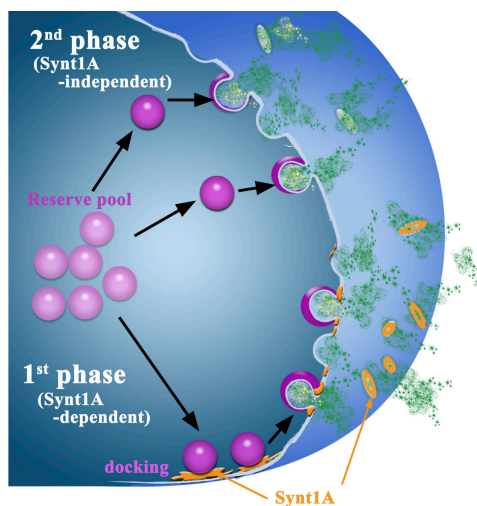
Figure 7. **Schematic drawing of the role of Synt1A in biphasic insulin release.** During first-phase insulin release, granules dock to Synt1A clusters and fuse at the site of Synt1A clusters. During second-phase release, granules move to the plasma membrane from the intracellular store and then fuse with the plasma membrane without any interaction with Synt1A clusters.

the plasma membrane in Synt1A$^{-/-}$ mice, it is difficult to conclude that both Synt3 and -4 are associated with first-phase exocytosis. Rather, we assume that the reduction of fusion events during the first phase by TAT-Synt3-H3 and TAT-Synt4-H3 treatment may reflect the homology of their amino acid sequence to Synt1A-H3. Nevertheless, it remains to be empirically determined if, and how, the other plasma membrane syntaxins contribute to the first phase.

Fusion from newcomer granules was not altered at all regardless of Synt1A deletion, indicating that this type of fusion may occur via some mechanism other than the Synt1A-based SNARE complex. Indeed, granule behavior between the first and second phases of release is quite different. As previously reported, upon reaching the plasma membrane, newcomers fused immediately ($<$50 ms), whereas granules previously docked on the plasma membrane stayed at the same place for a relatively long time (Ohara-Imaizumi et al., 2004b). To examine the possibility that other syntaxin isoforms are involved in second-phase exocytosis, we performed dominant-negative type experiments with TAT-Synt3-H3 and TAT-Synt4-H3 and demonstrated that there was no correlation between syntaxins and second-phase exocytosis. In agreement with our data, Spurlin and Thurmond (2006) noted only a slight decrease in second-phase insulin release in Synt4$^{+/-}$ mice. Thus, it is plausible that the first phase is Synt1A dependent but the second phase is Synt1A independent, as depicted in the Fig. 7. A similar phenomenon exists in neurotransmitter release, where neural t-SNARE SNAP-25 is essential for evoked neurotransmitter release but nonessential for nonevoked release (Washbourne et al., 2002). Furthermore, fusion via neural v-SNARE VAMP2 in evoked neurotransmitter release differs from spontaneous neurotransmitter release (Schoch et al., 2001). Of course, we do not know whether an evoked or spontaneous release in neurons is compatible with the first and second phases of insulin release in pancreatic β cells, respectively, but there must be some unknown

mechanism (other than the SNARE-mediated docking and fusion reactions) in different cell types. Further studies will be required to identify the specific molecules involved in newcomer fusion.

In the present study, we also examined the in vivo effect of Synt1A ablation followed by reduced first-phase insulin release on glucose homeostasis. The lack of first-phase insulin release is a main manifestation of type 2 diabetes (Ward et al., 1984; O'Rahilly et al., 1986; Cerasi, 1994). This phenomenon is quite similar to the insulin release pattern observed in the perfusion of Synt1A$^{-/-}$ β cells. Therefore, we expected Synt1A$^{-/-}$ mice to become diabetic. The in vivo studies showed that Synt1A$^{-/-}$ mice had impaired oral glucose tolerance and decreased serum insulin levels; however, there was no marked hyperglycemia. Thus, factors other than Synt1A depletion may be required to drive hyperglycemia. Williams-Beuren syndrome (Morris et al., 1988) is an interesting clinical case when considering the role of Synt1A in diabetes pathogenesis. This syndrome is a multi-system developmental disorder caused by the hemizygous deletion of a 1.5-million-bp region of chromosome 7q11.23 (Ewart et al., 1993), which includes the Synt1A gene (Osborne et al., 1997). Only some Williams-Beuren syndrome patients exhibit impaired glucose tolerance (Cherniske et al., 2004). This may be due to the hemizygous deletion; however, it is also postulated that deletion of only Synt1A is not enough to cause abnormal glucose homeostasis.

In summary, the present study has provided the first documentation that first-phase insulin release is Synt1A dependent, but second-phase release is Synt1A independent, highlighting that the two phases differ not only spatially but also mechanistically. In a physiological context, our data supporting glucose intolerance in Synt1A$^{-/-}$ mice in vivo encourage therapeutic consideration of the significance of Synt1A in first-phase insulin release.

Materials and methods

Generation of Synt1A$^{-/-}$ mice
We generated Synt1A$^{-/-}$ mice as previously described (Fujiwara et al., 2006). The genotyping of mice was performed by PCR. Mice were backcrossed with strain C57BL/6 over at least five generations and were used at the age of 10–14 wk. Animal experiments were approved by the Kyorin University Animal Care Committee.

Cells
Pancreatic islets of Langerhans were isolated from male WT and Synt1A$^{-/-}$ mice by collagenase digestion as described previously (Ohara-Imaizumi et al., 2004b). Isolated islets were dispersed in calcium-free Krebs-Ringer buffer (KRB) containing 1 mM EGTA and cultured on fibronectin-coated (KOKEN Co.), high refractive index cover glass (Olympus) in RPMI 1640 medium (Invitrogen) supplemented with 10% FBS (Invitrogen), 200 U/ml penicillin, and 200 μg/ml streptomycin at 37°C in an atmosphere of 5% CO_2. To label the insulin secretory granules, pancreatic β cells were infected with recombinant adenovirus Adex1CA insulin-GFP as described previously (Ohara-Imaizumi et al., 2004b). For Synt1A rescue experiments, cells were infected with Adex1CA Synt1A (Nagamatsu et al., 1999) before being infected with Adex1CA insulin-GFP. Experiments were performed 2 d after the final infection.

Immunoblotting
Proteins were extracted from mouse whole brain or mouse pancreatic islets and immunoblotted as previously described (Ohara-Imaizumi et al., 2005). Anti-Synt1A mAb and anti-Synt1B pAb were obtained also as previously

described (Fujiwara et al., 2006). Antibodies against Synt3 (Synaptic Systems GmbH), Synt4 (BD Biosciences), SNAP-25 (Wako), VAMP2 (Wako), and Munc18 (BD Biosciences) were purchased from commercial sources.

Immunostaining

WT and Synt1A$^{-/-}$ β cells cultured on high refractive index glass were fixed and made permeable with 2% paraformaldehyde/0.1% Triton X-100 and were processed for immunohistochemistry as described previously (Ohara-Imaizumi et al., 2004b). Cells were labeled with anti-insulin mAb (Sigma-Aldrich), Synt1A, and SNAP-25 and processed with goat anti–mouse IgG conjugated to Alexa Fluor 488 (Invitrogen; Ohara-Imaizumi et al., 2004b). Immunofluorescence was detected by TIRFM. This procedure allowed us to evaluate the number of docked insulin granules and clusters of Synt1A and SNAP-25.

EM

EM was performed by conventional methods as previously described (Akimoto et al., 1999). Tissues were fixed in phosphate-buffered 2.5% glutaraldehyde, pH 7.4, postosmicated, dehydrated with graded alcohols, and embedded in Epon 812. After staining with uranyl acetate and lead citrate, ultrathin sections were examined with a transmission electron microscope (TEM-1010C; JEOL). In EM, granules at their shortest distance of <10 nm from the plasma membrane were qualified as morphologically docked granules (Parsons et al., 1995).

Morphometric analysis of islets

For the analysis of islet size and β cell mass, paraffin-embedded pancreas sections (10 μm) were labeled with anti-insulin antibody and detected by an avidin-biotin-peroxidase technique (Vector Laboratories). Sections were collected at 500-μm intervals from tissue blocks, and all islets in the sections were analyzed as islet area over total pancreatic area. Images were acquired with a microscope (IX70; Olympus) that was equipped with a charge-coupled device (CCD) camera and analyzed with MetaMorph software (Universal Imaging Corp.).

TAT-conjugated antibody

TAT-conjugated Cy3-labeled anti-Synt1A antibody was prepared as described elsewhere (Ohara-Imaizumi et al., 2004a). In brief, anti-Synt1A mAb was labeled with Cy3 by use of a Fluoro Link antibody Cy3 labeling kit (GE Healthcare), according to the manufacturer's instructions. The Cy3-labeled antibody was dialyzed against 0.1 M borate buffer and was incubated with a fivefold molar excess of a cross-linker, sulfosuccinimidyl 6-(3'-[2-pyridyldithio]-propionamido) hexanoate (Pierce Chemical Co.) for 3 h at room temperature. The conjugated antibody was separated from the free cross-linker by gel filtration eluted with 5 mM Hanks' Hepes buffer, pH 7.2. A 10-fold molar excess of TAT protein transduction domain (PTD) peptide (GYGRKKRRQRRRGGGC) was added to the conjugated antibody, and the mixture was incubated overnight at 4°C. The TAT-conjugated antibody was separated from the free TAT PTD peptide by gel filtration eluted with 5 mM Hanks' Hepes buffer. On the day of TIRFM experiments, Adex1CA insulin-GFP–infected cells were treated with ~120 μg/ml TAT-conjugated Cy3-labeled anti-Synt1A mAb for 50 min as described previously (Ohara-Imaizumi et al., 2004a).

TAT fusion proteins

To produce constructs in which the TAT PTD peptide is located at the N terminus of Synt1A-H3 (aa 202–265), Synt1B-H3 (aa 201–264), Synt3-H3 (aa 201–264), Synt4-H3 (aa 210–273), or control peptides (non–coiled-coil domain of ELKS; aa 324–403; Ohara-Imaizumi et al., 2005), the coding region that corresponds to rat Synt1A-H3, Synt1B-H3, Synt3-H3, Synt4-H3, or control peptides was amplified by PCR by using oligonucleotide primers, including the nucleotide sequence against the TAT PTD peptide (YGRKKRRQRRR) in each sense primer, as described previously (Ohara-Imaizumi et al., 2002b). PCR products were subcloned into a pPROEX HTa bacterial expression vector (Invitrogen) with an additional His$_6$ tag at the N terminus. The resulting products were confirmed by an automated DNA sequencer (GE Healthcare). TAT fusion proteins in the pPROEX HTa vector were expressed in a DH5α *Escherichia coli* strain by induction with isopropyl-b-D-thiogalactopyranoside for 5 h at 37°C. The recombinant proteins were extracted with 8 M urea in 50 mM Tris and 100 mM KCl, pH 8.0. Urea extracts were incubated with Ni-NTA-agarose (QIAGEN) before washing, and stepwise removal of urea was performed to allow renaturation of bound protein. Proteins were eluted from Ni-agarose by 200 mM imidazole and were desalted on a PD-10 column (GE Healthcare) with Hanks' balanced salt solution (Invitrogen).

TIRFM

The Olympus total internal reflection system was used with a high-aperture objective lens (Apo 100× OHR; NA 1.65; Olympus) as previously published (Ohara-Imaizumi et al., 2002a). To observe GFP or Alexa Fluor 488 alone, we used a 488-nm laser line for excitation and a 515-nm long-pass filter for the barrier. Diiodomethane sulfur immersion oil (n = 1.81; Cargille Laboratories) was used to make contact between the objective lens and the high refractive index cover glass. Light propagates through the cover glass at an angle measured as 65° and undergoes total internal reflection at the glass–cell interface. The refractive indices for glass (n = 1.8 at 488 nm) and cells (n = 1.37) predict an evanescent field declining e-fold within 44 nm from the interface and to ~10% within 100 nm. A granule 100 nm from the interface would be illuminated too dimly to be visible under our conditions. Thus, we look barely 100 nm into the cell, a distance comparable to the thickness of ultrathin sections cut for EM (Zenisek et al., 2000). In an evanescent field declining e-fold within 44 nm, a granule at 80% brightness would have a vertical distance of 9.6 nm from the plasma membrane and qualify as a morphologically docked granule (granule distance from plasma membrane <10 nm in EM studies; Parsons et al., 1995). Images were projected onto a CCD camera (DV887DCSBV; Andor) operated with MetaMorph version 6.3. Images were acquired at 300-ms intervals. For real-time images of GFP-tagged insulin granule motion by TIRFM, treated β cells were placed on the high refractive index glass, mounted in an open chamber, and incubated for 30 min at 37°C in KRB containing 110 mM NaCl, 4.4 mM KCl, 1.45 mM KH$_2$PO$_4$, 1.2 mM MgSO$_4$, 2.3 mM calcium gluconate, 4.8 mM NaHCO$_3$, 2.2 mM glucose, 10 mM Hepes, pH 7.4, and 0.3% bovine serum albumin. Cells were then transferred to the thermostat-controlled stage (37°C) of TIRFM, and stimulation with glucose was achieved by the addition of 52 mM glucose-KRB into the chamber for a final concentration of 22 mM glucose. Most analyses, including tracking (single projection of different images) and area calculations were performed using MetaMorph software. To analyze the data, fusion events were manually selected, and the mean fluorescence intensity of individual granules in a 1 μm × 1 μm square placed over the granule center was calculated. The number of fusion events was manually counted while looping ~5,000 frame time lapses. To observe the fluorescence of GFP and Cy3 simultaneously, we used the 488-nm laser line for excitation and an image splitter (Optical Insight) that divided the green and red components of the images with a 565-nm dichroic mirror (Q565; Chroma Technology Corp.), passing the green component through a 530 ± 15 nm bandpass filter (HQ530/30 m; Chroma Technology Corp.) and the red component through a 630 nm ± 25 nm bandpass filter (HQ630/50 m [Chroma Technology Corp.]; Ohara-Imaizumi et al., 2005). Images were then projected side by side onto a CCD camera. The two images were brought into focus in the same plane by adding weak lenses to one channel, and they were brought into register by careful adjustment of the mirrors in the image splitter. Before each experimental session, we took an alignment image that showed density by means of scattered 90 nm TetraSpeck fluorescent beads (Invitrogen). They were visible in both the green and red channels, and thus provided markers in the x-y plane. Beads in the two images were brought into superposition by shifting one image using MetaMorph software.

Insulin release assay

β cells were housed in a small chamber (~5 × 10^5 cells/chamber) and perfused with KRB (2.2 mM glucose) for 60 min at a flow rate of 0.5 ml/min at 37°C before collecting fractions. Insulin release was stimulated by 22 mM glucose. Fractions were collected at 1-min intervals. Insulin release in aliquots of media was measured by an insulin ELISA kit (Morinaga).

Measurement of [Ca^{2+}]$_i$

β cells were loaded with 2 μM fura-2 acetoxymethyl ester (Fura-2 AM; Invitrogen) for 30 min at 37°C in KRB (2.2 mM glucose) and washed and incubated for an additional 15 min with KRB. Coverslips were mounted on an ARGUS/HiSCA system (Hamamatsu Photonics). Fura-2 fluorescence was detected by the cooled CCD camera after excitation at 340 nm (F340) and 380 nm (F380), and the ratio image (F340/F380) was calculated with the ARGUS/HiSCA system.

Oral glucose tolerance test

Male mice age 10–14 wk were fasted for 14–15 h before the test. Glucose was administered orally at 2 g glucose/kg body weight. Blood samples were collected from a tail vein at 0, 30, 60, 90, and 120 min after loading. Blood glucose levels were measured by Glutest R (Sanwa Kagaku Kenkyusyo). Plasma insulin levels were measured by an insulin ELISA kit.

References

Akimoto, Y., L.K. Kreppel, H. Hirano, and G.W. Hart. 1999. Localization of the O-linked N-acetylglucosamine transferase in rat pancreas. *Diabetes.* 48:2407–2413.

Bennett, M.K., N. Calakos, and R.H. Scheller. 1992. Syntaxin: a synaptic protein implicated in docking of synaptic vesicles at presynaptic active zones. *Science.* 257:255–259.

Cerasi, E. 1994. Aetiology of type II diabetes. *In* Insulin-Molecular Biology to Pathology. F.M. Ashcroft and S.J.H. Ashcroft, editors. IRL Press, Oxford, England. 352–392.

Cherniske, E.M., T.O. Carpenter, C. Klaiman, E. Young, J. Bregman, K. Insogna, R.T. Schultz, and B.R. Pober. 2004. Multisystem study of 20 older adults with Williams syndrome. *Am. J. Med. Genet. A.* 131:255–264.

Curry, D.L., L.L. Bennett, and G.M. Grodsky. 1968. Dynamics of insulin secretion by the perfused rat pancreas. *Endocrinology.* 83:572–584.

Ewart, A.K., C.A. Morris, D. Atkinson, W. Jim, K. Sternes, P. Spallone, A.D. Stock, M. Leppert, and M.T. Keating. 1993. Hemizygosity at the elastin locus in a developmental disorder, Williams syndrome. *Nat. Genet.* 5:11–16.

Fujiwara, T., T. Mishima, T. Kofuji, T. Chiba, K. Tanaka, A. Yamamoto, and K. Akagawa. 2006. Analysis of knockout mice to determine the role of HPC-1/syntaxin 1A in expressing synaptic plasticity. *J. Neurosci.* 26:5767–5776.

Gaisano, H.Y., C.G. Ostenson, L. Sheu, M.B. Wheeler, and S. Efendic. 2002. Abnormal expression of pancreatic islet exocytotic soluble N-ethylmaleimide-sensitive factor attachment protein receptors in Goto-Kakizaki rats in partially restored by phlorizin treatment and accentuated by high glucose treatment. *Endocrinology.* 143:4218–4226.

Henquin, J.C. 2000. Triggering and amplifying pathways of regulation of insulin secretion by glucose. *Diabetes.* 49:1751–1760.

Inoue, A., K. Obata, and K. Akagawa. 1992. Cloning and sequence analysis of cDNA for a neuronal cell membrane antigen, HPC-1. *J. Biol. Chem.* 267:10613–10619.

Jacobsson, G., A.J. Bean, R.H. Scheller, L. Juntti-Berggren, J.T. Deeney, P.O. Berggren, and B. Meister. 1994. Identification of synaptic proteins and their isoform mRNAs in compartments of pancreatic endocrine cells. *Proc. Natl. Acad. Sci. USA.* 91:12487–12491.

Jahn, R., and T.C. Südhof. 1999. Membrane fusion and exocytosis. *Annu. Rev. Biochem.* 68:863–911.

Jahn, R., T. Lang, and T.C. Südhof. 2003. Membrane fusion. *Cell.* 112:519–533.

Kang, Y., X. Huang, E.A. Pasyk, J. Ji, G.G. Holz, M.B. Wheeler, R.G. Tsushima, and H.Y. Gaisano. 2002. Syntaxin-3 and syntaxin-1A inhibit L-type calcium channel activity, insulin biosynthesis and exocytosis in beta-cell lines. *Diabetologia.* 45:231–241.

Lam, P.P., Y.M. Leung, L. Sheu, J. Ellis, R.G. Tsushima, L.R. Osborne, and H.Y. Gaisano. 2005. Transgenic mouse overexpressing syntaxin-1A as a diabetes model. *Diabetes.* 54:2744–2754.

Lang, T., M. Margittai, H. Holzler, and R. Jahn. 2002. SNAREs in native plasma membranes are active and readily form core complexes with endogenous and exogenous SNAREs. *J. Cell Biol.* 158:751–760.

Lizunov, V.A., H. Matsumoto, J. Zimmerberg, S.W. Cushman, and V.A. Frolov. 2005. Insulin stimulates the halting, tethering, and fusion of mobile GLUT4 vesicles in rat adipose cells. *J. Cell Biol.* 169:481–489.

Morris, C.A., S.A. Demsey, C.O. Leorard, C. Dilts, and B.L. Blackburn. 1988. Natural history of Williams syndrome: physical characteristics. *J. Pediatr.* 113:318–326.

Nagamatsu, S., T. Fujiwara, Y. Nakamichi, T. Watanabe, H. Katahira, H. Sawa, and K. Akagawa. 1996. Expression and functional role of syntaxin 1/HPC-1 in pancreatic β cells. *J. Biol. Chem.* 271:1160–1165.

Nagamatsu, S., Y. Nakamichi, C. Yamamura, S. Matsushima, T. Watanabe, S. Ozawa, H. Furukawa, and H. Ishida. 1999. Decreased expression of t-SNARE, syntaxin 1 and SNAP-25 in pancreatic beta-cells is involved in impaired insulin secretion from diabetic GK rat islets: restoration of decreased t-SNARE proteins improves impaired insulin secretion. *Diabetes.* 48:2367–2373.

O'Connor, V., C. Heuss, W.M. De Bello, T. Dresbach, M.P. Charlton, J.H. Hunt, L.L. Pellegrini, A. Hodel, M.M. Burger, H. Betz, et al. 1997. Disruption of syntaxin-mediated protein interactions blocks neurotransmitter secretion. *Proc. Natl. Acad. Sci. USA.* 94:12186–12191.

Ohara-Imaizumi, M., Y. Nakamichi, T. Tanaka, H. Ishida, and S. Nagamatsu. 2002a. Imaging exocytosis of single insulin secretory granules with evanescent wave microscopy: distinct behavior of granule motion in biphasic insulin release. *J. Biol. Chem.* 277:3805–3808.

Ohara-Imaizumi, M., Y. Nakamichi, C. Nishiwaki, and S. Nagamatsu. 2002b. Transduction of MIN6 beta cells with TAT-syntaxin SNARE motif inhibits insulin exocytosis in biphasic insulin release in a distinct mechanism analyzed by evanescent wave microscopy. *J. Biol. Chem.* 277:50805–50811.

Ohara-Imaizumi, M., C. Nishiwaki, T. Kikuta, K. Kumakura, Y. Nakamichi, and S. Nagamatsu. 2004a. Site of docking and fusion of insulin secretory granules in live MIN6 beta cells analyzed by TAT-conjugated anti-syntaxin 1 antibody and total internal reflection fluorescence microscopy. *J. Biol. Chem.* 279:8403–8408.

Ohara-Imaizumi, M., C. Nishiwaki, T. Kikuta, S. Nagai, Y. Nakamichi, and S. Nagamatsu. 2004b. TIRF imaging of docking and fusion of single insulin granule motion in primary rat pancreatic beta-cells: different behaviour of granule motion between normal and Goto-Kakizaki diabetic rat beta-cells. *Biochem. J.* 381:13–18.

Ohara-Imaizumi, M., T. Ohtsuka, S. Matsushima, Y. Akimoto, C. Nishiwaki, Y. Nakamichi, T. Kikuta, S. Nagai, H. Kawakami, T. Watanabe, and S. Nagamatsu. 2005. ELKS, a protein structurally related to the active zone-associated protein CAST, is expressed in pancreatic beta cells and functions in insulin exocytosis: interaction of ELKS with exocytotic microscopy. *Mol. Biol. Cell.* 16:3289–3300.

O'Rahilly, S.P., A.S. Rudenski, M.A. Burnett, Z. Nugent, J.P. Hosker, and P. Darling. 1986. Beta-cell dysfunction rather than insulin insensitivity is the primary defect in familial type 2 diabetes. *Lancet.* 2:360–364.

Osborne, L.R., S. Soder, X.M. Shi, B. Pober, T. Costa, S.W. Scherer, and L.C. Tsui. 1997. Hemizygous deletion of the syntaxin 1A gene in individuals with Williams syndrome. *Am. J. Hum. Genet.* 61:449–452.

Ostenson, C.G., A. Khan, S.M. Abdel-Halim, A. Guenifi, K. Suzuki, Y. Goto, and S. Efendic. 1993. Abnormal insulin secretion and glucose metabolism in pancreatic islets from the spontaneously diabetic GK rat. *Diabetologia.* 36:3–8.

Ostenson, C.G., H. Gaisano, L. Sheu, A. Tibell, and T. Bartfai. 2006. Impaired gene and protein expression of exocytotic soluble N-ethylmaleimide attachment protein receptor complex proteins in pancreatic islets of type 2 diabetic patients. *Diabetes.* 55:435–440.

Parsons, T.D., J.R. Coorssen, H. Horstmann, and W. Almers. 1995. Docked granules, the exocytic burst, and the need for ATP hydrolysis in endocrine cells. *Neuron.* 15:1085–1096.

Rorsman, P., and E. Renstrom. 2003. Insulin granule dynamics in pancreatic beta cells. *Diabetologia.* 46:1029–1045.

Rorsman, P., L. Eliasson, E. Renstrom, J. Gromada, S. Barg, and S. Gopel. 2000. The cell physiology of biphasic insulin secretion. *News Physiol. Sci.* 15:72–77.

Saito, T., S. Okada, E. Yamada, K. Ohshima, H. Shimizu, K. Shimomura, M. Sato, J.E. Pessin, and M. Mori. 2003. Syntaxin 4 and Synip (syntaxin 4

interacting protein) regulate insulin secretion in the pancreatic βHC-9 cell. *J. Biol. Chem.* 278:36718–36725.

Schoch, S., F. Deaf, A. Konigstorfer, M. Mozhayeva, Y. Sara, T.C. Südhof, and E.T. Kavalali. 2001. SNARE function analyzed in synaptobrevin/VAMP knockout mice. *Science.* 294:1117–1122.

Spurlin, B.A., and D.C. Thurmond. 2006. Syntaxin 4 facilitates biphasic glucose-stimulated insulin secretion from pancreatic beta-cells. *Mol. Endocrinol.* 20:183–193.

Südhof, T.C. 2004. The synaptic vesicle cycle. *Annu. Rev. Neurosci.* 27:509–547.

Ward, W.K., D.C. Bolgiano, B. McKnight, J.B. Halter, and D. Porte Jr. 1984. Diminished β-cell secretory capacity in patients with non-insulin dependent diabetes mellitus. *J. Clin. Invest.* 74:1318–1328.

Washbourne, P., P.M. Thompson, M. Carta, E.T. Costa, J.R. Mathews, G. Lopez-Bendito, Z. Molnar, M.W. Becher, C.F. Valenzuela, L.D. Partridge, and M.C. Wilson. 2002. Genetic ablation of the t-SNARE SNAP-25 distinguishes mechanisms of neuroexocytosis. *Nat. Neurosci.* 5:19–26.

Wheeler, M.B., L. Sheu, M. Ghai, A. Bouquillon, G. Grondin, U. Waller, A.R. Beaudoin, M.K. Bennett, W.S. Trimble, and H.Y. Gaisano. 1996. Characterization of SNARE protein expression in β cell lines and pancreatic islets. *Endocrinology.* 137:1340–1348.

Yang, S.N., O. Larsson, R. Branstrom, A.M. Bertorello, B. Leibige, I.B. Leibiger, T. Moede, M. Kohler, B. Meister, and P.O. Berggren. 1999. Syntaxin 1 interacts with the L(D) subtype of voltage-gated Ca^{2+} channels in pancreatic beta cells. *Proc. Natl. Acad. Sci. USA.* 96:10164–10169.

Zenisek, D., J.A. Steyer, and W. Almers. 2000. Transport, capture and exocytosis of single synaptic vesicles at active zones. *Nature.* 406:849–854.

Zhang, W., A. Khan, C.G. Ostenson, P.O. Berggren, S. Efendic, and B. Meister. 2002. Down-regulated expression of exocytotic proteins in pancreatic islets of diabetic GK rats. *Biochem. Biophys. Res. Commun.* 291:1038–1044.

Zhong, P., Y.A. Chen, D. Tam, D. Chung, R.H. Scheller, and G.P. Miljanich. 1997. An alpha-helical minimal binding domain within the H3 domain of syntaxin is required for SNAP-25 binding. *Biochemistry.* 36:4317–4326.